MULTI-FREQUENCY STUDY OF SUPERNOVA REMNANTS AND H II REGIONS IN NGC300

J. L. Payne
Centre for Astronomy, James Cook University
Townsville, QLD, 4811, Australia
JEFFREY.PAYNE@JCU.EDU.AU
M. D. Filipović, T. G. Pannuti, P. A. Jones
M.FILIPOVIC@UWS.EDU.AU, TPANNUTI@IPAC.CALTECH.EDU, PAUL.JONES@ATNF.CSIRO.AU
N. Duric, G. L. White, S. Carpano
DURIC@UNM.EDU, GRAEME.WHITE@JCU.EDU.AU, CARPANO@ASTRO.UNI-TUEBINGEN.DE

Abstract

We present a multi-frequency study of supernova remnants (SNRs) and H II regions in the nearby Sculptor Group Sd galaxy NGC300, based on new ATCA observations at the wavelengths of 13 and 20 cm, *XMM-Newton* observations, newly-processed *ROSAT* (PSPC/HRI; Read & Pietsch 2001) and VLA (20/6 cm) images of this galaxy. We have investigated the physical properties at the X-ray and radio wavelengths of the 28 optical SNRs found by Blair & Long (1997) and have expanded on the multi-wavelength work by Pannuti et al. (2000) on this same galaxy. From a total of 54 radio sources and 11 X-ray sources, we report 18 SNRs and five (5) SNR candidates (classified by spectral index alone) in NGC300. Five of these 18 SNRs are associated with reported optical SNRs and three have X-ray counterparts. An additional 12 radio SNRs are seen in the Blair & Long (1997) [S II] images. We also investigate luminosity function of our SNRs. Three background radio sources are confirmed and 12 other sources could represent additional background objects. Twenty two radio correlations with OB associations within NGC300 correspond to either H II regions or SNRs making them a good tracer of SNRs near star-forming regions. Additionally, two of our radio sources coincide with potential globular clusters of NGC300 reported by Kim et al. (2002).

1 Introduction

While many SNRs located within the Milky Way Galaxy have been extensively studied (see for example, the recent multi-wavelength study of the Galactic SNR 3C397; Dyer & Reynolds 1999), such work has been hampered by factors such as massive photoelectric absorption along the plane of the Galaxy at short wavelengths, as well as significant uncertainties in distances to SNRs (and corresponding diameter uncertainties). In addition, the position of the Sun within the Galactic disk and toward its edge makes it difficult to completely sample all of the Galactic SNRs.

To address these difficulties, observers have searched for SNRs in nearby galaxies. However, such optical observations need to be complemented by observations at other wavelengths in order to both detect a maximum number of SNRs in a galaxy of interest and to locate SNRs at all stages of their evolution.

As pointed out in Lacey & Duric (2001), there may be a selection effect inherent in optical surveys, which are more sensitive to detecting SNRs away from H II regions. Such SNRs may be weak emitters in the X-ray and radio because of their location within low density environments. In contrast, SNRs that are powerful sources of X-ray and radio emission are often located within H II regions. It is precisely because of their location in H II regions that they may be missed by optical surveys.

2 Observations

Observations reported here are:

1. ATCA radio-continuum observations on 28 Feb 2000 in the 6C antenna configuration at 1374 and 2496 MHz achieving a resolution of $6''$.

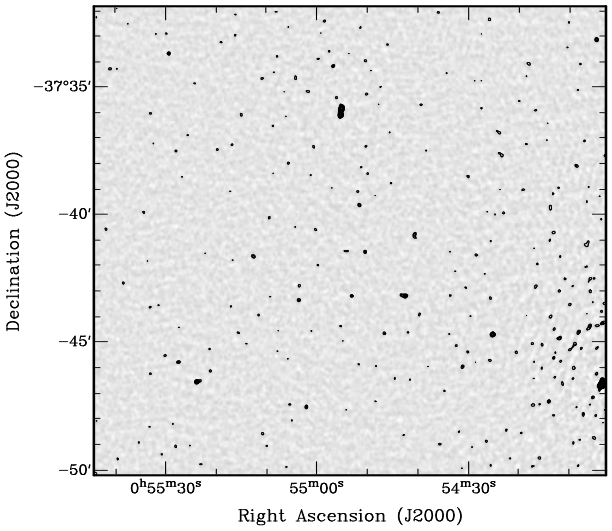

Figure 1: The ATCA 2496 MHz image of NGC300 with its contours. Contours are: 0.2, 0.3, 0.4, 0.5, 0.7, 1, 1.5, 2, 3, 4 and 5 mJy.

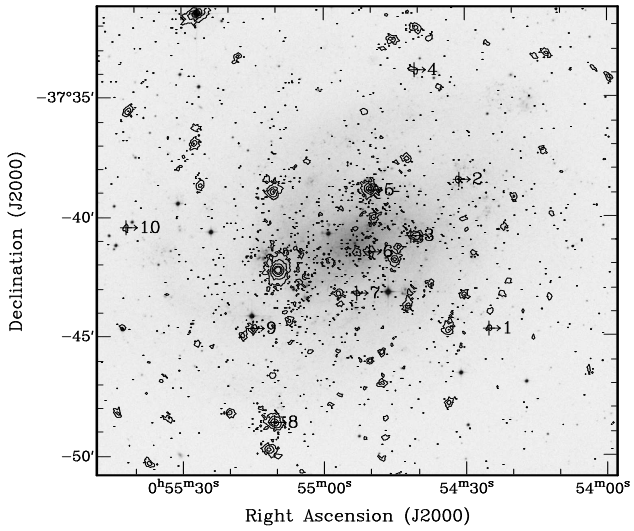

Figure 2: *XMM-Newton* (energy range 0.3–6.0 keV) image (contours) of NGC300 overlaid on DSS2-Red (R) image (gray scale). Radio identifications are marked and X-ray contours are: 7, 21, 63, 190 and 380 counts.

2. *XMM-Newton* observations in Dec 2000 ($\sim$ 37 ks) and Jan 2001 ($\sim$ 47 ks) utilizing the EPIC MOS1, MOS 2 and PN detectors with a medium filter.

3. VLA radio-continuum observations at 6 cm (resolution $8.63'' \times 4.22''$) on 22 May 1993 and at 20 cm (resolution $4.70'' \times 3.76''$) on 13 Jun 1998 in CnB and BnA configurations, respectively. After reductions, the effective frequencies were 4860 MHz (6 cm) and 1448 MHz (20 cm).

4. Reprocessed *ROSAT* images from several pointed observations between 1991 and 1997 as reported by Read & Pietsch (2001).

3 Reduction and analysis

Radio data was reduced using the MIRIAD, AIPS and KARMA suite of programs; X-ray data reduction was accomplished using *XMM-Newton*'s SAS and HEAsoft's XSPEC. Figure 1 shows the ATCA 2496 MHz image of NGC300 with contours.

We found sensitivity values of 0.058, 0.066, 0.062 and 0.037 mJy for frequencies of 1374, 1448, 2496 and 4860 MHz, respectively. Assuming a distance of 2.02 Mpc (Freedman et al., 2001), this corresponds to luminosity limits of 2.83×10^{16}, 3.22×10^{16}, 3.03×10^{16} and 1.81×10^{16} W Hz^{-1}.

For each frequency of our data, the MIRIAD software package task IMSAD was used to detect all sources above a flux cutoff, taken as 3σ. We used IMFIT to determine the flux density of our selected sources by marking a region around each at 3σ rms.

We assume all radio images have a positional accuracy of less than $1''$ and utilizing the viewer in the KARMA software package (Gooch, 1996), sources were selected using multi-frequency contour levels and catalog annotation files overlaying a DSS2-Red (R) image of the galaxy. Using information from the NASA/IPAC Extragalactic Database (Jet Propulsion Laboratory, California Institute of Technology and National Aeronautics and Space Administration), an ellipse ($21.9' \times 15.5'$) overlay centered on the galaxy at RA(J2000) = $00^{\rm h}54^{\rm m}53.48^{\rm s}$ Dec(J2000) = $-37°41'3.8''$ provided a visual boundary. A grid annotation file allowed systematic visualization of each source field such that no region would be missed.

Positional identifications with published sources in the optical and X-ray domains were considered high if they fell within the positional limits of these surveys ($\sim 4''$). An exception was the *ROSAT* catalog created by Read & Pietsch (2001) who cite positional errors for each of their X-ray sources individually.

We show *XMM-Newton* sources that identify with our radio sources in Table 1 and Fig. 2. These were chosen visually by comparing overlapping contours from the *XMM-Newton* and all four radio images using the KARMA software package.

Table 1: *XMM-Newton* sources found to match our radio sources showing PN detector hardness ratios and count rates. A complete catalog of *XMM-Newton* sources can be found in Carpano (in prep.). Col. 4 abbreviation Pe represents the estimated positional error

(1)	(2)	(3)	(4)	(5)			(6)		
Source Number	RA (J2000)	Dec (J2000)	Pe	Revolution 192			Revolution 195		
(XMMU)	h m s	° ′ ″	(″)	Tot (count ks^{-1})	HR1	HR2	Tot (count ks^{-1})	HR1	HR2
XMM1 / J005425.2−374441	00 54 25.20	−37 44 41.1	0.9	1.13	−0.26	−1.00	1.47	−0.13	−0.25
XMM2 / J005431.4−373827	00 54 31.45	−37 38 27.0	0.7	0.62	−0.01	−0.60	1.76	+0.04	−0.19
XMM3 / J005441.6−374048	00 54 41.69	−37 40 48.0	1.5	1.27	−0.63	−0.99	1.63	−0.58	−1.00
XMM4 / J005440.8−373351	00 54 40.85	−37 33 51.3	0.8	1.39	+0.84	+0.94	0.72	+0.31	+0.62
XMM5 / J005450.0−373853	00 54 50.08	−37 38 53.2	0.1	28.39	+0.31	+0.11	20.62	+0.35	+0.19
XMM6 / J005450.4−374128	00 54 50.45	−37 41 28.4	0.6	2.02	−0.48	−0.92	2.23	−0.64	−1.00
XMM7 / J005453.2−374311	00 54 53.21	−37 43 11.8	0.8	0.88	−0.34	+0.79	1.27	−0.35	+0.02
XMM8 / J005510.7−374835	00 55 10.75	−37 48 35.8	0.3	27.16	−0.37	−0.75	29.83	−0.43	−0.73
XMM9 / J005515.2−374439	00 55 15.27	−37 44 39.6	0.4	5.36	−0.69	−0.95	0.93	−1.00	−0.98
XMM10 / J005542.0−374025	00 55 42.04	−37 40 25.6	0.7	2.35	−0.76	−0.88	1.08	−0.88	−0.93

For point like X-ray sources with greater than 200 counts per observation, we were able to fit simple spectral models to the combined data for each observation using `XSPEC` after grouping the data to a minimum of 25 counts. Using this technique, we fitted a spectrum to two X-ray sources; XMMU J005450.0−373853 and XMMU J005510.7−374835 (our XMM5 and XMM8, respectively). The best spectral fit for XMM5 was a photoelectric absorption with bremsstrahlung model although the photoelectric absorption with power law model was a nearly as good. For XMM8, the best fit was clearly the photoelectric absorption with power law model.

Spectral fitting was more difficult for sources having few counts (< 200). For these sources, we used hardness ratios to give some indication of their X-ray spectra. Using our energy bands: soft (0.3–1.0 keV), medium (1.0–2.0 keV) and hard (2.0–6.0 keV); HR1 was defined as the ratio of the difference of medium and soft counts to their sum ((med−soft)/(med+soft)). In similar fashion, HR2 was defined as the ratio of the differences of hard and soft counts to their sum ((hard−soft)/(hard+soft)). Table 1 shows the results of these calculations for data obtained from the PN detector for each observation.

Simulated models of "fake" sources show that hardness ratios tend to be negative for thermal objects and positive for non-thermal ones. This only gives a rough estimate of our source's X-ray spectra. We cannot always assume that SNRs have a thermal X-ray spectrum as noted, for example, by the discovery of non-thermal emission from SN1006 (Koyama et al., 1997).

The nature of radio objects within our ellipse centered on NGC300 was determined using radio spectral index (determined by calculating the line of best fit for our flux densities to find α[1]), *XMM-Newton* observations and catalog identifications. Because of distance (2.02 Mpc), we could not use radio source extension or morphology as part of our criteria.

Catalogs used include; 28 optical SNRs identified by Blair & Long (1997) based on [S II]:Hα ratios of 0.4 or greater, H II regions found by Deharveng et al. (1988) (176) and Soffner et al. (1996) (90), 117 OB associations published by Pietrzyński et al. (2001), 17 globular cluster candidates found by Kim et al. (2002) and X-ray observations of the galaxy reported by Read & Pietsch (2001). We also used original Blair & Long (1997) ([S II] and Hα) images and DSS2-Red (R) plates to help validate our sources.

Our selection criteria may be summarized as follows:

1. **For Background Sources:** If a source with a very steep spectral index ($\alpha \leq -0.8$) was found to have an identification in the X-ray domain, it was designated as a background source or "BKG". If no spectral index could be calculated because the source was too faint at other radio wavelengths, then catalog identifications were used to determine if the source *could* be a background object. If no resolution using this information was possible, these sources were not designated. Sources with a steep radio spectral index but no other identifications were designated as "bkg" as were those

[1] defined by $S_\nu \propto \nu^\alpha$, where S_ν is the integrated flux density and ν is frequency

sources with a flat spectral index (due to the possible variability of background sources in general). We adopted the estimate given by Pannuti et al. (2000) that approximately five background sources should have been observed in random directions through the disk of NGC300 in the VLA 20 cm image at a 3σ level of 0.2 mJy or greater. (They based their estimate on work by Mitchell & Condon (1985) for the number density of background sources.)

2. **For H II Regions:** Sources described in other catalogs as H II regions were designated as "HII". Those with a flat radio spectral index that did not have identifications at other wavelengths or catalog descriptions were listed as "hii/bkg". The "hii" designation was required because DSS2-Red (R) or Hα images may not have been sensitive enough to show these potential H II regions. The "bkg" designation was included since these radio sources *could* be intrinsically variable with flat indexes. Sources with a steeper (or borderline steeper) spectral index which were described as both H II regions (and possible supernova remnants) in other catalogs were designated as "SNR/HII" since these most likely represent areas where a supernova remnant was embedded within or associated with an H II region. Most of these sources could be visually seen in BL97 [S II] images as discussed below, although this alone did not classify the objects.

3. **For Supernova Remnants:** In addition to SNRs embedded within H II regions, a source known to be a supernova remnant from other catalogs was designated as "SNR" in Table 2. Our classification of a radio SNR candidate, "snr†" was based on spectral index when no identifications were found and did not include those sources that could have been a supernova remnant while just as likely another type of source, such as a background object. For example, ATCA J005525.8−373653 could be either a supernova remnant or background source and was designated as "snr/bkg". This source was not included in our count of SNR candidates. In fact, any source that has radio and X-ray emission unexplained otherwise had "snr" (possible supernova remnant) as one of its possible designations.

We list in Table 2, for each of 54 detected radio objects; source number, position (RA and Dec), integrated flux densities (1374, 1448, 2496 and 4860 MHz), spectral index with standard error where more than two points were used, source type, rough comparisons to Blair & Long (1997) images and identifications with sources at other wavelengths.

3.1 Calibrations

We compared our ATCA (1374 MHz) and VLA (1448 MHz) flux densities, expecting that a spectral index as high as -2 would predict a mean ratio of 1.11 (with ATCA fluxes higher). Instead, we found a mean ratio of 1.44. While we argue that elevation differences during VLA ($\sim 18°$) and ATCA ($\sim 75°$) observations could account for this, there are too many other possible factors. This may include differences in instrumentation, exposure times and reduction technique.

The scatter in the resulting spectral index for each source is reflected in its standard error listed in Table 2. Errors in spectral index are too great to be used alone for source typing. This is the reason we use it as only one of several factors to characterize our sources.

We also compared the positions of 16 H II regions cited in Deharveng et al. (1988) to their ATCA counterparts at 1374 MHz and have found no significant positional bias between our radio positions and the optical positions. At the 95 percent confidence level (using the student-t with n-1 degrees of freedom), the positional differences in right ascension and declination ($\Delta\alpha$ and $\Delta\delta$, respectively) are $\Delta\alpha = -0.7'' \pm 0.7$, $\Delta\delta = -0.5'' \pm 0.8$. Comparisons of 1374 MHz positions with positions at the other radio frequencies and *XMM-Newton* show the radio catalogs to be self-consistent.

4 Sources

4.1 Supernova remnants

4.1.1 Statistics of SNRs

We attempted to create a brightness-diameter relation for our radio SNRs that have measured (optical) diameters (Blair & Long, 1997). As there were only five of these, no meaningful conclusion from this comparison could be made.

We also found that the average 1374 MHz luminosity of our radio SNRs was 2.26×10^{17} W Hz^{-1}, just above the 5σ completeness level of 1.4×10^{17} W Hz^{-1}. No

Table 2: Measured radio-continuum properties of objects within NGC300. Listed positions (RA and Dec) are from 1374 MHz observations where possible. In Col. 10, visual comparisons are made to BL97 [S II] versus Hα (with some contamination from [N II]) images; 0=no flux, VF=very faint flux, F=faint flux, M=medium flux and S=strong flux. Prefixes to source numbers used in Col. 11: H=HRI (Read & Pietsch, 2001), P=PSPC (Read & Pietsch, 2001), D=Deharveng et al. (1988), S=Soffner et al. (1996), DSS2-Red(f/m)=STScI Digitized Sky Survey (1993,1994), BL=Blair & Long (1997), RPS97=Read et al. (1997), PSNR=Pannuti et al. (2000), GC=Kim et al. (2002), AS_=Pietrzyński et al. (2001) and XMM=This paper. Source type abbreviations are: SNR=supernova remnant, HII=H II-region, BKG=background object and xrb=X-ray binary (capital letters denote higher confidence). †– denotes snr candidates

1 ATCA Source Number	2 RA (J2000) h m s	3 Dec (J2000) ° ′ ″	4 $S_{1374MHz}$ (mJy)	5 $S_{1448MHz}$ (mJy)	6 $S_{2496MHz}$ (mJy)	7 $S_{4860MHz}$ (mJy)	8 $\alpha \pm \Delta\alpha$	9 Source Type	10 [S II]/Hα (BL)	11 Identifications
J005408.6−373804	00 54 08.69	−37 38 04.7			0.76					DSS2-Red(f)
J005422.5−373615	00 54 22.53	−37 36 15.1	0.53						0/VF	
J005423.4−373741	00 54 23.48	−37 37 41.4	0.47	0.40	0.56		$+0.4 \pm 0.3$	hii/bkg	0/0	
J005423.8−373648	00 54 23.84	−37 36 48.4	0.74	0.54	0.54		-0.3 ± 0.5	snr†	0/0	
J005423.8−373621	00 54 23.88	−37 36 21.1	0.46						0/0	
J005425.2−374441	00 54 25.25	−37 44 41.9	2.71	2.57	2.22	0.20	-2.0 ± 0.6	BKG		XMM1
J005431.2−374554	00 54 31.28	−37 45 54.6	0.58	0.39	0.58		$+0.3 \pm 0.6$	hii/bkg		
J005431.9−373825	00 54 31.91	−37 38 25.9	0.40					SNR	F/F	P29(HR2=0.15), BL-S6([S II]/Hα=0.60), XMM2,AS_18
J005437.9−374559	00 54 37.99	−37 45 59.5	0.70	0.54	0.28		-1.4 ± 0.3	bkg	0/0	
J005438.1−374144	00 54 38.16	−37 41 44.2	0.32	0.38		0.11	-0.9 ± 0.2	SNR/HII	F/S	S(west)31, D39,DSS2-Red(f),PSNR2(R1),AS_25
J005438.4−374240	00 54 38.49	−37 42 40.5		0.25				snr/HII	F/F	D40,PSNR3(R2), RPS97(no. 2),AS_26a
J005439.6−373543	00 54 39.61	−37 35 43.4	0.55	0.42	0.38		-0.4 ± 0.4	snr†	0/0	
J005440.6−374049	00 54 40.68	−37 40 49.7	0.71	0.32	0.54	0.26	-0.5 ± 0.5	SNR/HII	M/M	P38(HR2=-0.33), BL-S10([S II]/Hα=0.67), XMM3,H11,S(west)22,DSS2-Red(f),AS_29
J005441.0−373348	00 54 41.05	−37 33 48.9	0.38	0.35				bkg/snr	0/0	XMM4
J005442.7−374313	00 54 42.70	−37 43 13.3	0.88	0.61	0.87	0.30	-0.7 ± 0.4	SNR/HII	M/S	D53B,DSS2-Red(m), BL-S11([S II]/Hα=0.53),AS_34
J005443.1−374311	00 54 43.11	−37 43 11.0	0.66	0.48	0.53	0.43	-0.2 ± 0.2	SNR/HII	M/S	D53A,PSNR4(R3),DSS2-Red(s),AS_34
J005445.3−373842	00 54 45.31	−37 38 42.8				0.18		HII	0/0	D62,AS_45
J005445.3−373847	00 54 45.39	−37 38 47.1	0.42		0.28		-0.7	SNR/HII	F/S	D61,DSS2-Red(m),AS_45
J005448.0−373323	00 54 48.01	−37 33 23.7	0.40	0.34					0/0	DSS2-Red(f)
J005450.2−374030	00 54 50.28	−37 40 30.0		0.74		0.14	-1.4	SNR/HII	M/S	D76A,PSNR7(R6),DSS2-Red(m),AS_56
J005450.3−373822	00 54 50.30	−37 38 22.4	0.46	0.23	0.30	0.27	-0.2 ± 0.3	SNR/HII	M/S	D77,DSS2-Red(m),AS_52a
J005450.3−373850	00 54 50.35	−37 38 50.9	0.29					xrb	M/F	DSS2-Red(f)P32(HR2=0.75),H10, XMM5,AS_52
J005450.5−374123	00 54 50.52	−37 41 23.0	0.38	0.29	0.45		$+0.5 \pm 0.5$	hii/bkg	0/0	XMM6
J005450.7−374022	00 54 50.73	−37 40 22.2	0.21			0.14	-0.3	SNR/HII	F/F	DSS2-Red(f),D76B,AS_56b
J005450.8−374015	00 54 50.82	−37 40 15.1				0.15		HII	VF/VF	D76B,AS_56b
J005451.1−373826	00 54 51.16	−37 38 26.1	0.40	0.24		0.14	-0.6 ± 0.3	SNR/HII	M/S	D79,DSS2-Red(m),AS_52d
J005451.3−374621	00 54 51.34	−37 46 21.9		0.24				HII	VF/S	PSNR10(R9),D82,DSS2-Red(f)
J005451.7−373939	00 54 51.79	−37 39 39.6	0.48	0.49	0.48	0.38	-0.2 ± 0.1	SNR/HII	M/S	DSS2-Red(s),D84, PSNR11(R10),GC6,AS_57
J005453.3−374311	00 54 53.30	−37 43 11.9	0.82	0.59	0.44	0.12	-1.4 ± 0.3	BKG	M/F	DSS2-Red(m),XMM7,GC7
J005455.3−373557	00 54 55.32	−37 35 57.5	17.59	17.27	9.54	1.86	-1.8 ± 0.3	bkg	0/0	
J005456.3−373940	00 54 56.36	−37 39 40.0	0.57	0.34				HII	M/F	DSS2-Red(m),D99
J005456.7−373413	00 54 56.77	−37 34 13.8	0.37	0.35	0.59		$+0.9 \pm 0.2$	hii/bkg	0/0	
J005500.5−374037	00 55 00.58	−37 40 37.4	0.27		0.33	0.12	-0.7 ± 0.5	SNR/HII	F/S	DSS2-Red(m),D109,S(east)20,AS_76
J005500.7−374143	00 55 00.73	−37 41 43.5	0.26					HII	VF/S	DSS2-Red(f),S(east)19,D111
J005500.9−373720	00 55 00.93	−37 37 20.1	0.28	0.30	0.36		$+0.4 \pm 0.1$	hii/bkg	0/0	
J005501.4−373829	00 55 01.49	−37 38 29.9	0.41		0.28		-0.6	SNR	0/0	AS_82
J005502.1−373952	00 55 02.13	−37 39 52.4	0.42						0/0	
J005502.2−374731	00 55 02.25	−37 47 31.0	0.48	0.27	0.60		$+0.8 \pm 0.9$	hii/bkg	0/0	
J005503.5−374246	00 55 03.50	−37 42 46.0	0.47	0.33	0.36	0.30	-0.2 ± 0.2	SNR/HII	F/S	DSS2-Red(m), D118A,PSNR12(R11),AS_84
J005503.6−374320	00 55 03.66	−37 43 20.1	0.50	0.36	0.47	0.18	-0.6 ± 0.3	SNR/HII	M/S	D119A,DSS2-Red(m), PSNR13(R12),AS_86
J005507.3−374106	00 55 07.30	−37 41 06.1				0.12		HII	VF/M	DSS2-Red(f),D126,S(east)4,AS_94
J005510.8−374835	00 55 10.85	−37 48 35.3	0.69	0.31	0.55		$+0.2 \pm 1.2$	AGN		DSS2-Red(f),P58(HR2=0.01), H16,XMM8
J005512.3−373908	00 55 12.37	−37 39 08.5			0.26			HII	0/F	DSS2-Red(f),D136
J005512.7−374140	00 55 12.70	−37 41 40.3	0.68	0.29	0.54	0.26	-0.4 ± 0.5	SNR/HII	M/S	DSS2-Red(m), PSNR14(R13),D137A,AS_102b
J005515.4−374439	00 55 15.40	−37 44 39.2	0.24	0.22	0.38		$+0.9 \pm 0.2$	SNR/HII	S/S	D141,P49(HR2=-0.16),XMM9, BL-S26([S II]/Hα=0.57),DSS2-Red(f), AS_107
J005516.4−374653	00 55 16.45	−37 46 53.7	0.40					VF/VF		
J005521.3−374609	00 55 21.35	−37 46 09.6	0.90	0.44	0.48		-0.6 ± 1.0	snr†	0/0	
J005523.9−374632	00 55 23.95	−37 46 32.4	3.06	1.70	1.71		-0.6 ± 0.9	snr†	0/0	
J005525.8-373653	00 55 25.82	−37 36 53.8	0.74	0.59	0.42		-0.8 ± 0.3	bkg/snr		
J005527.6−374546	00 55 27.66	−37 45 46.4	0.49	0.31	0.73		$+1.0 \pm 0.8$	hii/bkg		
J005528.2−374903	00 55 28.25	−37 49 03.3	1.05	0.76	0.68		-0.5 ± 0.5	snr†		
J005533.6−374147	00 55 33.65	−37 41 47.8			0.39			HII	0/F	D158,DSS2-Red(f)
J005533.8−374314	00 55 33.87	−37 43 14.6	0.38					SNR/HII	M/S	D159,BL-S28([S II]/Hα=0.61), DSS2-Red(f),AS_113
J005541.9−374033	00 55 41.94	−37 40 33.5			0.60			snr	0/0	P36(HR2=-0.26),XMM10

meaningful conclusions could be made since we have selected for only the brightest SNRs in NGC300.

4.1.2 Optically selected SNRs

Of the five Blair & Long (1997) SNRs that identify with our sources, two (BL-S10 and BL-S11) have radio spectral indexes consistent with SNRs. Two sources (BL-S6 and BL-S28) have no spectral index while the other (BL-S26) is inverted. Additionally, three of these BL97 sources (BL-S6, BL-S10 and BL-26) have corresponding X-ray emission. We also find that as many as three Blair & Long (1997) optical SNRs have X-ray emission but no radio detection. As noted by Chen & Chu (1998), only a small number of optically identified extragalactic SNRs can be confirmed at radio and X-ray wavelengths with these being among the most luminous remnants.

Blair & Long (1997) notes that while the canonical value of 0.4 in the ratio of [S II] to Hα has worked well in the Milky Way and Local Group galaxies to separate shock-heated nebulae from photoionized gas, the exact value of this cutoff has not been important since there is a gap in the distribution. Photoionized regions tend to show a ratios of ~ 0.2 or below. In Col. 10 of Table 2 we show the results of a visual inspection of original 1500s plates from BL97. Although not quantitative, we see [S II] emission from 12 sources other than the SNRs reported by them. H II regions without an SNR identification tend to show little or no [S II] emission.

An example of an interesting object not reported in Blair & Long (1997) because it fell below the [S II]:Hα ratio cutoff is ATCA J005438.1−374144 (Fig. 3). In this object, the typical spherical shape of a SNR can be seen with a diameter of about 70 pc in the [S II] image. Radio emission (with a resolution of $6''$ compared to an optical resolution of $1.5''$) is seen from the most intense area at '4 o'clock', highlighting that non-thermal radio emission from SNRs appear to be formed at the shock. In fact, the expanding shell of a SNR may be undergoing different processes at the same time causing some areas to emit non-thermal radio radiation while other regions do not.

Radio emission from what appears to be a shell shock front are also seen in at least two other radio SNRs and less defined shells are noted in six more. We cannot determine the [S II]:Hα ratios of the above sources from existing Blair & Long (1997) observations since these images were only used to screen for SNRs candidates which were further studied by directed optical long-slit CCD spectral techniques.

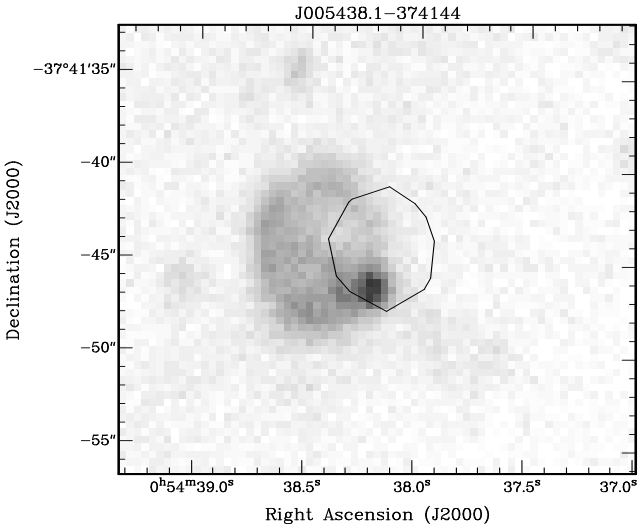

Figure 3: ATCA J005438.1−374144 radio SNR with 0.174 mJy radio contour superimposed on Blair & Long (1997) [S II] optical image ($1'' = 10.2$ pc).

4.1.3 Radio selected SNRs

We found thirteen additional SNRs than reported by Blair & Long (1997) based on radio spectral index and identification with H II regions or OB associations (Table 2). Although most of them have some optical emission as discussed above, there is a general lack of X-ray emission from this group of objects.

SNR ATCA J005451.7−373939 has a positional identification with both a globular cluster (GC6) and an OB association. It seems likely in this case, the radio emission is associated with the OB association and that the globular cluster is simply superimposed since cluster SNRs most likely have dissipated into the interstellar medium long ago.

4.2 Other interesting sources

We find three background sources based on positional identifications and spectral index. Although most of these sources represent distant galaxies, one of these, ATCA J005453.3−374311, is coincident with another globular cluster reported by Kim et al. (2002). Its X-ray color and radio spectral index is consistent with a power law spectrum.

ATCA J005425.2−374441 also has a very steep spectral index of -2.0, but its X-ray color (XMM1) is a bit softer. Still, it is certainly possible that this object also

has a X-ray power law spectrum as evidenced by its X-ray color proximity to ATCA J005510.8−374835, which clearly corresponds to an AGN as reported by Read & Pietsch (2001). Using *XMM-Newton* data, we were able to fit a photoelectric absorption power law model to the latter.

ATCA J005450.3−373850 is possibly associated with an X-ray binary[2] (P32; our XMM5) as reported by Read & Pietsch (2001) which they base on its distance of 30″ from the nearest SNR and its HR2 value of 0.75. Using HRI data, they also found a 41% probability that the X-ray source is variable. We have labeled this source "xrb" since the spectrum we found is also consistent with their conclusion. Our X-ray model fit shows the object to have a photoelectric absorption Bremsstrahlung spectrum. However, the photoelectric absorption power law fit is also very good. Perhaps this object has both thermal and power law properties. Its radio emission may be the result of synchrotron emission from jets, making this a rare example of a microquasar. Only one other suspected extragalactic microquasar has been reported by Dubus (2003) (in the nucleus of M33). We expect this type of source to be rarely found in extragalactic studies since detection of its relatively faint radio emission is unlikely at these distances.

5 Discussion and conclusions

Pannuti et al. (2000) could place only limits on the radio spectral indexes from eight of their 14 radio sources because they had only one flux density (λ = 20 cm) for each of them. Our findings support six SNRs identifications they made for radio sources having VLA flux densities at both 6 and 20 cm wavelengths. We also find a 6 cm flux for their R1, allowing us to agree with a total of seven. While we disagree with the remainder of their SNR identifications, the addition of ATCA fluxes in the 13 and 20 cm wavelength range allow us to find an additional six.

In summary, out of a total of 54 radio sources and 11 X-ray sources, we have found and described 18 SNRs in NGC300; 13 in addition to those found in the optical by Blair & Long (1997). Three of the five SNRs identified by Blair & Long (1997) that have radio counterparts also have X-ray counterparts. We find evidence for [S II] emission from an additional 12 of our radio sources, implying that a total of 17 SNRs have some optical component.

There are five additional SNR candidates in NGC300 which will await further studies for verification. These sources do not appear to have any optical component, although ATCA J005528.2−374903 is not within the boundary of the Blair & Long (1997) images.

All identifications with *ROSAT* sources are included in our *XMM-Newton* X-ray identifications with radio sources except source number 2 (coincident with Pannuti et al. (2000) R2) reported in Read et al. (1997). Although this source could be a supernova remnant also, we do not have a radio spectral index.

While it has been understood that many SNRs lie embedded within H II regions, we also note a strong correlation of our radio sources near 22 OB associations within this galaxy. All of our 18 radio SNRs identify with an OB association.

We also find the expected number of background sources within the region covered by NGC300. An additional seven *XMM-Newton* X-ray sources match our radio sources other than the SNRs mentioned above. Three are identified with background objects and one is associated with a likely X-ray binary as discussed above. Two X-ray sources *could* be background objects while one identifies with another X-ray supernova candidate (P36) discussed in Read & Pietsch (2001).

Acknowledgments

We thank Wolfgang Pietsch and Andy Reid for allowing us to use their *ROSAT* image of NGC300 for our analysis. TGP would like to thank the staff of the ATNF for their hospitality during the observing run. We also used the `KARMA` software package developed by the ATNF and the `EXSAS/MIDAS` software package developed by the MPE.

We also thank William Blair who graciously provided us with the images of NGC300 used in Blair & Long (1997). These Los Campanas Observatory observations were transferred from tape at our request.

DSS2-Red (R) plates were based on photographic data obtained using the UK Schmidt Telescope. The Digitized Sky Survey was produced at the Space Telescope Science Institute (STScI) under US Government grant NAG W-2166.

[2] X-ray emission from accretion onto a compact star from a normal star in a binary system

References

Blair, W. P., Long, K. S. 1997, ApJS, 108, 261 (BL97)
Chen, C. H. R., Chu, Y.-H. 1998, AAS, 193.7405C
Deharveng, L., Caplan, J., Lequenx, J., Azzopardi, M., Breysacher, J., Tarenghi, M., Westerlund, B. 1988, A&AS, 73, 407
Dubus, G. 2003, in *Semaine de l'Astrophysique Franaise, EdP-Sciences, Conference Series*, eds. Combes, F., Barret, D. & Contini, T., Bordeaux, France, 202
Dyer, K. K., Reynolds, S. P. 1999, ApJ, 526, 365
Freedman, W. L., et al. 2001, ApJ, 553, 47F
Gooch, R. 1996, ADASS, 5, 80
Kim, S. C., Sung, H., Lee, M. G. 2002, JKAS, 35, 9
Koyama, K., Kinugasa, K., Matsuzaki, K., Nishiuchi, M., Sugizaki, M., Torii, K., Yamauchi, S., Aschenbach, B. 1997, PASJ, 49L, 7K
Lacey, C. K., Duric, N. 2001, ApJ, 560, 719
Mitchell, K. J., Condon, J. J. 1985, AJ, 90, 1957
Pannuti, T. G., Duric, N., Lacey, C. K., Goss, W. M., Hoopes, C. G., Walterbos, R. A. M., Magnor, M. A. 2000, ApJ, 544, 780
Pietrzyński, G., Gieren, W., Fouqué, P., Pont, F. 2001, A&A, 371, 497
Read, A. M., Pietsch, W. 2001, A&A, 373, 473
Read, A. M., Ponman, T. J., Strickland, D. K. 1997, MNRAS, 286, 626
Soffner, T., Meńdez, R. H., Jacoby, G. H., Ciardullo, R. Roth, M. M., Kudritzki, R. P. 1996, A&A, 306, 9S